Science
AAAS

Supplementary Materials for

NIN-like protein 7 transcription factor is a plant nitrate sensor

Kun-Hsiang Liu *et al*.

Corresponding authors: Kun-Hsiang Liu, khliu@molbio.mgh.harvard.edu; Jen Sheen, sheen@molbio.mgh.harvard.edu

Science **377**, 1419 (2022)
DOI: 10.1126/science.add1104

The PDF file includes:

Other Supplementary Material for this manuscript includes the following:

Materials and Methods

Plasmid constructs and transgenic lines

To generate NLP1-9 expression plasmids for transient expression assays in mesophyll protoplasts, the NLP1,2,4,5,6,7,8,9 coding regions were PCR amplified from *Arabidopsis* cDNA and the NLP3 was PCR amplified from genomic DNA, and then inserted into the plant expression vector with a constitutive promoter *pHBT-HA-NOS* plasmid (*18, 36, 37*). The NLP7 point mutations in the plant expression plasmids were generated by site-directed mutagenesis (*38*). *N-NLP7* and *NLP7-C* were generated by PCR and cloned into the *pHBT-HA-NOS* vector. *LjNIN* was amplified from the *pHBT-LjNIN-cMYC-NOS* plasmid (*25*) and cloned into the *pHBT-HA-NOS* vector. To generate *pHBT-N-NLP7-NIN-C-HA-NOS* and *pHBT-N-NIN-NLP7-C-HA-NOS* plasmids, *N-NIN* and *NLP7-C* or *N-NLP7* and *NIN-C* fragments were PCR amplified from *pHBT-LjNIN-HA-NOS* and *pHBT-NLP7-HA-NOS* plasmids and cloned into the *pHBT-HA-NOS* plasmid using In-Fusing cloning (Vazyme). To complement *nlp7* with *pNLP7:NLP7-mEGFP* or *pNLP7:NLP7(HLY/AAA)-mEGFP*, the 2 kb promoter fragment of *NLP7* was amplified from genomic DNA and the coding region of *NLP7-mEGFP* or *NLP7(HLY/AAA)-mEGFP* were amplified from *pHBT-NLP7-mEGFP-NOS* or *pHBT-NLP7(HLY/AAA)-mEGFP-NOS,* and cloned into the *pCAMBIA1300* binary vector (www.cambia.org). The plasmids were transformed into *nlp7* mutant plants using the *Agrobacterium* GV3101(*pSoup-p19*)-mediated floral-dip method (*39, 40*). At the T3 generation, homozygous single-copy insertion lines were selected for analyses.

The plant nitrate-responsive reporter *4xNRE-min-LUC* was generated by replacing the *NIR* promoter in *pNIR-LUC* (*18*) with synthesized *4xNRE-min* promoter DNA fragment (table S4) (*25*). The internal control *pCAMV-RLUC-CAMV* DNA fragment was inserted next to *4xNRE-min-LUC* in the same plasmid. To generate *Human-4xNRE-min-LUC*, *4xNRE* was synthesized (Tsingke, China) and cloned into the *pGL4.23* plasmid with a mammalian minimal promoter (*min*) and the *SV40* terminator (Addgene, Cat no.: 60323). The herpes simplex virus-*TK-Renilla* Luciferase (*pHSV-TK-RLUC-SV40*) plasmid was used as an internal control (Promega).

To obtain the *pCMV-MYC-NLP7-mEGFP-β–Globin* plasmid, *mEGFP* coding region was cloned into the *pCMV-MYC-β–Globin* plasmid, and then PCR-amplified *NLP7* coding region from *HBT-NLP7-HA-NOS* was inserted into *pCMV-MYC-mEGFP-β–Globin*. To generate *pCMV-MYC-OsNLP3-mEGFP-β–Globin*, PCR-amplified coding region of *OsNLP3* from rice cDNA (*Oryza sativa*) was inserted into *pCMV-MYC-mEGFP-β–Globin.* The *pCMV-MYC-OsNLP3(HLY/AAA)-mEGFP-β–Globin* plasmid was generated by inserting mutated *OsNLP3(HLY/AAA)* after side-directed mutagenesis.

To generate *pHBT-NLP7-mEGFP-NOS*, the *NLP7* fragments was amplified by PCR from *pHBT-NLP7-HA-NOS* and cloned into the *pHBT-mEGFP-NOS* plasmid. To obtain *pHBT-NLP7(RRKKK/AAAAA)-mEGFP-NOS*, *pCMV-NLP7(RRKKK/AAAAA)-mEGFP-SV40* was first created by site-directed mutagenesis to avoid competition with the endogenous nuclear NLP7. The NLP7(RRKKK/AAAAA) fragment was then amplified from *pCMV-NLP7(RRKKK/AAAAA)-mEGFP-SV40* by PCR and cloned into *pHBT-mEGFP-NOS* plasmid. To create the *sCiNiS* plasmid, PCR-amplified *NLP7(RRKKK/AAAAA)* DNA fragment from *pCMV-NLP7(RRKKK/AAAAA)-mEGFP-SV40,* was first cloned into a synthesized plasmid *pCMV-mCitrine* (Tsingke, China) after digestion with BamHI to generate the plasmid with split *N-mCitrine-NLP7(RRKKK/AAAAA)-mCitrine-C* (table S4) (*41*). The split *N-mCitrine-NLP7(RRKKK/AAAAA)-mCitrine-C* DNA fragment was amplified by PCR and inserted into the *pUBQ10-HA-NOS* plasmid to generate *pUBQ10-N-mCitrine-NLP7(RRKKK/AAAAA)-mCitrine-C-NOS* (*sCiNiS*). To obtain *sCiNiS* for plant transformation, the *pUBQ10-N-mCitrine-NLP7(RRKKK/AAAAA)-mCitrine-C-NOS* fragment was amplified by PCR and inserted into the binary vector *pGIIB-p35S-LIC-NOS* (*42*). The *sCiNiS* transgenic plants were generated using the *Agrobacterium* GV3101*(pSoup-p19)*-mediated floral-dip method (*39, 40*). Transgenic plants were selected by spraying with BASTA herbicide.

To generate plasmids carrying *GST-NLP7-8xHIS, GST-N-NLP7-8xHIS, GST-*

NLP7(HLY/AAA)8xHIS and *GST-N-NLP7(HLY/AAA)-8xHIS* for protein expression in *E. coli*, the coding regions were amplified from *pHBT-NLP7-HA-NOS* and *pHBT-NLP7(HLY/AAA)-HA-NOS* and cloned into the *pGEX-4T-2* plasmid (GE Healthcare). All plasmids were validated by sequencing. The primers used for plasmid constructions are listed in table S5. The synthesized DNA plasmid sequences are listed in table S4.

Plant materials and growth conditions

Arabidopsis ecotype Columbia (Col-0) was used as the wide type (WT). The *chl1-5* mutant was a gift from Yi-Fang Tsay. The *nlp7-1* null mutant (named *nlp7* in this article) was obtained from *Arabidopsis* Biological Resource Centre. For RNA-seq analysis of endogenous NLP target genes, each NLP was transiently overexpressed in mesophyll protoplasts (with nitrate signaling for activating NLPs) isolated from WT plants (leaf 5-6, the third pair of true leaves) grown at 23/20 °C, 12 h/12 h light/dark, 60% RH, and 75 μmol m^{-2} s^{-1}mol of light for 4 weeks in soils (small Jiffy pellet). To examine and compare the shoot development phenotypes in WT, *chl1-5,* and *nlp2,4,5,6,7,8,9*, plants were grown at 23°C, 12 h/12 h light/dark, 60% RH, and 70 μmol m^{-2} s^{-1}mol of light in the soil (Pindstrup) for 16 days. The shoots were collected for the acquisition of images (Canon DOS80D). To monitor plant growth in response to different nitrogen sources, around 20 seedlings were germinated and grown on the Petri dish (150 mm X 15 mm) containing 100 ml of nitrogen-free 1xMS medium salt (Caisson), 0.1% MES, 1% sucrose, 0.7% phytoagar (PlantMedia), supplemented with 2.5 mM ammonium succinate or 5 mM KNO_3, pH 5.8 at 23°C, 12h /12h light/dark, 70 μmol m^{-2} s^{-1} of light for 15 days. Photos were taken using a digital camera (Canon DOS80D) and processed using Adobe Photoshop (Adobe). To monitor root morphology in response to nitrate, seedlings were germinated and grown on a basal medium supplemented with 2.5 mM ammonium succinate and 1% phytoagar under constant light (150 μmol m^{-2} s^{-1}) at 23 °C for 3 days. Plants were then transferred to the basal medium supplemented with 5 mM KNO_3, and grown for 8 days. To measure the

primary and lateral root length, pictures were taken using a digital camera (Canon DOS80D) and processed using Adobe Photoshop (Adobe), and then analyzed by ImageJ. To obtain nitrate-free mesophyll protoplasts, around 23-30 plants were germinated and grown on the Petri dish (150 mm X 15 mm) containing the nitrate-free medium described above and supplemented with 2.5 mM ammonium succinate as the sole nitrogen source under 23℃, 12h /12h light/dark, 70 μmol m^{-2} $s^{-1}$of light for 24-28 days. Mesophyll protoplasts were isolated from the second and the third pair of true leaves following the mesophyll protoplast isolation protocol (*37*).

For RNA-seq analysis of the primary nitrate responses in WT, *chl1-5*, and *nlp2,4,5,6,7,8,9*, 10 seedlings were germinated in one well of the 6-well tissue culture plate(Falcon) with 1 ml of the basal medium (10 mM KH_2PO_4/K_2HPO_4, 1 mM $MgSO_4$, 1 mM $CaCl_2$, 0.1 mM $FeSO_4$-EDTA, 50 μM H_3BO_4, 12 μM $MnSO_4 \cdot H_2O$, 1 μM $ZnCl_2$, 1 μM $CuSO_4 \cdot 5H_2O$, 0.2 μM $Na_2MoO_4 \cdot 2H_2O$, 0.1% MES and 0.5% sucrose, pH 5.8) supplemented with 2.5 mM ammonium succinate as the sole nitrogen source. Plates were sealed with parafilm under constant light (100 μmol m^{-2} s^{-1}) at 23℃ for 7 days. The medium was refreshed on day 6. Before nitrate induction, seedlings were washed three times with 1 ml basal medium without nitrogen. Seedlings were induced in 1 ml of basal medium with 10 mM KCl or KNO_3 for 20 min. Seedlings were harvested for RNA extraction with TRIzol (Thermo Fisher Scientific). For nitrate uptake assay (*24*), 10 seedlings were germinated in one well of the 6-well tissue culture plate (Corning) with 1 ml of ammonium succinate basal medium as described above under constant light (45 μmol m^{-2} s^{-1}) at 23℃ for 7 days.

For gene expression analyses with RT-qPCR of *pNLP7-NLP7-mEGFP* and *pNLP7-NLP7(HLY/AAA)-mEGFP* complementation lines, 10 seedings were germinated in one well of the 6-well tissue culture plate with 1 ml of the basal medium supplemented with 2.5 mM ammonium succinate as the sole nitrogen source. Plates were sealed with parafilm and placed under constant light (45 μmol m^{-2} s^{-1}) at 23℃ for 6 days. On day 6, seedlings were washed three times with 1 ml basal medium. Seedlings were then

incubated in 1 ml of basal medium without nitrogen source for 1 day. Nitrate induction at day 7, seedlings were treated in 1 ml of basal medium with 10mM KCl or KNO_3 for 2 h. Seedlings were then harvested for RNA extraction with TRIzol (Thermo Fisher Scientific).

For gene expression analyses with RT-qPCR of WT seedlings in response to chlorate, 10 seedings were germinated in one well of the 6-well tissue culture plate with 1 ml of the basal medium supplemented with 2.5 mM ammonium succinate as the sole nitrogen source. Plates were sealed with parafilm and placed under constant light (45 μmol m-2 s-1) at 23 °C for 7 days. Seven-day-old wild-type seedlings were washed with 1 ml basal medium, and seedlings were treated with 10 mM KCl or 10 mM KNO_3, or 10 mM $KClO_3$ for 15 min. Seedlings were then harvested for RNA extraction with TRIzol (Thermo Fisher Scientific).

For sCiNiS imaging, transgenic seedlings were germinated and grown in a 6-well tissue culture plate with 1 ml of ammonium succinate basal medium as described above under 12 h/12 h light/dark photoperiod at 23°C for 5 days.

Transient expression assays in leaf cells

Mesophyll protoplasts isolation from true leaves of soil-grown or culture-medium-grown plants was previously described (*18, 37*). For RNA-seq analysis experiments, mesophyll protoplasts (10^6 protoplasts in 5 ml) from soil-grown plants were transfected with 500 μg *HBT-NLP-HA-NOS* or an empty vector plasmid and incubated in WI buffer for 4.5 h (*18*). The expression levels of NLP-HA in protoplasts were monitored by immunoblot analysis with anti-HA-peroxidase (Roche, 11667475001; 1:1,000). In general, protein expression was first detectable 2-3 h after DNA transfection. The endogenous target genes activated by each NLPs are involved in primary nitrate responses (*15-16, 18-19, 21*).

The *NRE-LUC* activity in response to nitrate induction was performed in nitrate-free mesophyll protoplasts (2 x 10^4 protoplasts in 100 μl) isolated from wild type, *nlp6*,

nlp7-1, *nlp6,7-1*, *nlp2,4,5,6,7,8,9* transfected with 10 μg *4xNER-min-RLUC* plasmid and incubated in WI buffer for 4 h and then induced by 10 mM KCl or KNO_3 for 2 h. The dual luciferase (LUC and RLUC) assay was carried out according to the manufacturer's protocol using a dual luciferase reporter gene assay kit (Yeasen, Cat no.:11402ES60). For NLP7-mEGFP and NLP7(RRKKK/AAAAA)-mEGFP localization analysis, mesophyll protoplasts (2 x 10^4 protoplasts in 200 μl) were co-transfected with 7.5 μg of *pHBT-mEGFP-NOS* or *pHBT-NLP7(RRKKK/AAAAA)-mEGFP-NOS* and 7.5 μg of *pHBT-HY5-mCherry* (*18*) as a nuclear marker control. Protoplasts were incubated in WI buffer for 12 h. The image was recorded via the ECHO software on the ECHO Revolve microscope (ECHO) with the 10X objective lens. The images were processed using Adobe Photoshop software.

To investigate the functions of NLP7, LjNIN, N-NLP7, NLP7-C, N-NLP7-NIN-C, N-NIN-NLP7-C, and the NLP7 mutants generated by alanine scanning mutagenesis in nitrate signaling, nitrate-free mesophyll protoplasts from plants grown on ammonium-succinate culture medium were co-transfected with 10 μg *4xNER-min-RLUC* plasmid and 10 μg of a different plasmid expressing various NLP or NIN protein and incubated in WI buffer for 4 h for protein expression. Protoplasts were then induced with low 0.5 mM KCl or KNO_3 for 2 h. The protein expression levels in protoplasts were monitored by immunoblot analysis with anti-HA-peroxidase (AB, Cat no.:11667475001; 1:1,000).

Transient expression assays in 293T human cells

293T cells were maintained in Dulbecco's modified Eagle's medium (Gibco, USA) supplemented with 10% (v/v) FBS and 5% (v/v) CO_2 at 37°C. For transient transfection, 293T cells were transferred to 6-well cell culture plates and incubated at 5 % (v/v) CO_2 and 37°C for 24 h. The transfection was performed using the modified PEI-max method (*43*). Briefly, 2 μg *pCMV-MYC* plasmid harboring a different gene, 0.5 μg *human4xNRE-min-LUC,* and 0.25 μg *HSV-RLUC* plasmid were mixed into 150

μL Opti-MEM (Gibco, USA), and then added 8.25 μL PEI-max (1 μg/μL pH 7.0) to make a mixture. The mixture was incubated for 5 min at room temperature before adding to the cells. Transfected 293T cells were incubated for 6 h and then induced with 10 mM KCl or KNO_3 for 2 h. Transfected 293T cells were washed with PBS buffer and the luciferase activity was detected by a dual luciferase reporter gene assay kit (Yeasen, Cat no.:11402ES60). The expression levels of MYC-tagged protein in 293T cells were monitored by immunoblot analysis with an anti-MYC antibody (MBL, Cat no.: M192-3, 1:2,000).

RNA-Seq analysis

Putative target genes of each NLPs were identified in WT mesophyll protoplasts from soil-grown plants by transiently overexpressing individual NLP genes for 4.5 h. Samples from two biological replicates were processed in three batches including three separate vector-only controls. Total RNA (0.5 μg) was used to generate the libraries as previously described using the NEBNext® Ultra II™ RNA Library Prep Kit for Illumina® sequencing (NEB, Cat no.: E7760) (*18*). The libraries were sequenced on an Illumina Hi-seq 2500 with the single-end, 50 bp reads mode. Library sequencing was performed at Tufts University Core Facility (Boston, USA). The sequencing result was analyzed as described previously (*18*). Briefly, differentially expressed genes were determined with DESeq2 comparing NLP versus control. Results were imported into Microsoft Excel for filtering ($Log_2 \geq 1$ or ≤ -1, $P < 0.05$ cut-off). To generate a heatmap, agglomerative hierarchical clustering on genes with Gene Cluster 3.0 using Correlation (uncentred) as the similarity metric and centroid linkage as the clustering method. Java Treeview was used to visualize the results of the clustering.

For RNA-seq analysis of the primary nitrate responses in WT, *chl1-5,* and *nlp2,4,5,6,7,8,9,* total RNA (0.5 μg) isolated from 7-d seedlings was used for preparing the library with NEBNext® Ultra II™ RNA Library Prep Kit for Illumina® sequencing according to the manufacturer's guidelines. The libraries were sequenced using a

NextSeq 2000 at MGH Next Generation Sequencing Core Facility (Boston, USA) with a pair-end, 50 bp reads mode. The sequencing result was analyzed as previously described (*18*). Differentially expressed genes were determined for WT KNO_3 (N) versus WT KCl (K) and *nlp2,4,5,6,7,8,9* KNO_3 (N) versus *nlp2,4,5,6,7,8,9* KCl (K).

qRT-PCR

RNA isolation, and RT-qPCR were performed as described previously (*18*). First-strand cDNA was synthesized from 1 µg of total RNA using the UEIris RT mix with Dnase (All-in-One) reverse transcription system (US Everbright, Cat. No.: R2020) in a total volume of 20 µl. Real-time RT-PCR was carried out by CFX96 real-time PCR-detection system (Biorad) using SYBR green Master Mix (US Everbright, Cat. No.: S2014). For each PCR reaction, 0.5 µl of the reverse transcription reaction was used. The sequences of primers are listed in table S6. The relative gene expression was normalized to the expression of *UBQ10*.

HTSeq data analysis

For gene expression analyses from RNA-seq experiment in WT, *chl1-5,* and *nlp2,4,5,6,7,8,9* seedlings, HTSeq read counts of *UBQ10*, *NIA1, NIA2, UPM1, NRT2.1, NRT3.1, LBD37, LBD38, LBD39, CBF2, TGA1, MAPKKK14, G6PD3,* and *FNR2,* genes were analyzed using Microsoft Excel software. The relative gene expression was normalized to the expression of *UBQ10*. The fold change was calculated relative to the value of WT treated with KCl.

Nitrate uptake measurement

Seven-day-old WT, *chl1-5* or *nlp2,4,5,6,7,8,9* seedlings grown in the ammonium-succinate basal medium were washed with 1 ml basal medium without nitrogen 3 times. The seedlings were shifted to a basal medium supplemented with 1 mM KNO_3. Samples of the solution were taken from the well at 0, 20 min and 1 h, and

the fresh weight of seedlings was calculated. The nitrate concentration was determined by High Pressure Ion Chromatography (HPIC) using a Dionex IonPac AS11-HC column (Thermo Scientific).

Protein expression and purification from *E. coli*

Each expression plasmid was transformed into Rosetta 2 (DE3) pLysS competent Cells (Novagen). Cells were induced by 0.5 mM of isopropyl-B-thiogalactopyranoside (IPTG) when OD_{600} reached 0.6, and proteins were expressed at 18 ℃ for 18 h. Bacteria were harvested by centrifugation. The cell pellet was resuspended in 100 ml of lysis/wash buffer (1 X PBS buffer supplement with proteinase inhibitor (cOmplete mini, Roche), 50 mM imidazole, and 1 mM DTT) and cells were disrupted a Qsonica sonicator (Sino sonics). The lysate was centrifuged (15,000xg, 15 min, 4 ℃) and the supernatant was transferred to a 50 ml falcon tube. One ml of equilibrated Ni-NTA agarose (Qiagen) was added to lysate and mixed by rotating at 4℃ for 60 min. The lysate-Ni-NTA agarose mixture was loaded into a 10 ml poly-prep chromatography column (Bio-rad, Cat no.: 7311550). The Ni-NTA agarose in the column was washed three times with 10 ml lysis/wash buffer. The protein was eluted 4 times with 0.5 ml elution buffer (1 X PBS, 250 mM imidazole, and 1 mM DTT). The elute protein (2 ml) was subject to the second step of purification by adding 10 ml GST bind/wash buffer (140 mM NaCl, 2.7 mM KCl, 10 mM Na_2HPO_4, 1.8 mM KH_2PO_4, pH 7.4) and 1 ml of equilibrated GST resin (EMD Millipore, Cat no.: 70541) was added. NLP7 protein and GST resin were rotated at 4 ℃ for 30 min. The lysate-GST resin mixture was loaded into a 10 ml poly-prep chromatography column. The GST resin in the column was washed three times with 10 ml GST bind/wash buffer. The protein was eluted 4 times with 0.5 ml elution buffer (50 mM Tris-HCl pH 7.5, 10 mM Glutathione reduced form). Purified proteins were buffer exchanged into buffer containing 1 X PBS and 1 mM DTT and concentrated by Amicon ultra centrifugal filter united with Ultracel-10 membrane (EMD Millipore). One μg of each purified protein was loaded

and separated in 7.5 % SDS-Page gel. The gel was stained using a ready blue protein gel stain system (Sigma-Aldrich, Cat no.: RBS-1L) according to the user guide.

MicroScale Thermophoresis (MST) analysis

The MST assay was performed by the NanoTemper monolith NT.115 instrument (*29, 44*). The purified GST-NLP7-8xHIS, or GST-N-NLP7-8xHIS, or GST-NLP7(HYL/AAA)-8xHIS, or GST-N-NLP7(HYL/AAA)-8xHIS or HIS-GST (Prospec, Cat no.:ENZ-451) was labeled by His-Tag Labeling (The Monolith His-Tag Labeling Kit RED-tris-NTA 2nd Generation kit) (NanoTemper Technologies) in assay buffer (20 mM HEPES buffer pH 7.5, 1 mM DTT and 0.005 % Tween-20) at room temperature for 30 min. A series of dilutions of KNO_3, $KClO_3$, or KPO_4 (K_2HPO_4 + KH_2PO_4, pH 7.0) with 5 nM labeled protein. The experiments were carried out using 10 % LED power and 80 % MST for purified proteins and 5 % LED power and 20 % MST for HIS-GST protein. K_d was calculated using a quadratic binding equation via Nano Temper software from triplicate experiments.

Surface Plasmon Resonance (SPR) analysis

SPR analyses were performed with a CM5 sensor chip (Cytiva, Cat no.:BR100012) on a Biacore T200 instrument (GE Healthcare) at Harvard Medical School, Center for macromolecular interactions. Purified GST-N-NLP7-8xHIS, GST-N-NLP7(HYL/AAA)-8xHIS or HIS-GST protein was buffer-exchanged to 10 mM sodium acetate buffer (pH 5.0). Immobilization of protein was performed using an amine coupling kit (Cytiva, Cat no. BR-1000-50) at 25°C (*30*). The purified proteins were captured at ~ 3,000-7,000 response units (RU) and HIS-GST was captured at ~12,000-15,000 response units (RU), and a blank channel was used as a blank surface reference. KNO_3, $KClO_3$, or KPO_4 (K_2HPO_4 + KH_2PO_4, pH 7.0) was diluted in HBSP buffer (150 mM NaCl, 10 mM HEPES, 0.05 % Tween 20, pH 7.4) to indicated concentrations and injected at a flow rate of 50 µl min^{-1} for 60 s, followed by

dissociation for 2 min. All SPR data processing and analyses were performed using BiaEvaluation Software (version 3.0). All binding resonance signals were presented after double-reference (blank surface reference and blank buffer reference) correction. The steady-state binding curve was fitted using the 1:1 Langmuir binding mode to obtain the K_d value.

The design of genetically encoded nitrate biosensor sCiNiS

Biosensor design is often empirical and best supported by 3D structural information. Although the structure of the nitrate-binding pocket is predictable (Fig. 5C), how nitrate triggers the conformational change of full-length NLP7 remained to be elucidated. It is possible that the full-length NLP7 would be sufficiently large and flexible with the nitrate-binding domain (395-438 aa) sitting near the middle to facilitate the reconstitution of full mCitrine protein from N-mCitrine and mCitrine-C after nitrate binding. As suggested in Chardin et al., 2014 (*17*), the putative GAF motifs of NLP proteins are located upstream of the conserved nitrate-binding domain (395-438 aa in NLP7) (Fig. 4A and Fig. 5, A and B). When only the N-NLP7 domain was used, the nitrate-binding site would be located at the C-terminus and N-NLP7 might be too rigid to bring the N-mCitrine and mCitrine-C together in proximity for the reconstitution of full mCitrine protein after nitrate binding.

sCiNiS-based nitrate confocal imaging in transgenic seedlings

Five-day-old seedlings were grown in a nitrate-free medium. A chamber was made on microscope slides with two strips of invisible tape (50 mm × 24 mm) and filled with 40 µl of the basal medium. The 5-day-old seedling was embedded in the medium. A thin layer of cotton fiber was placed on top of the cotyledon. The coverslip (24 mm × 24 mm) was placed on the sample and fixed by another two strips of invisible tape. Confocal imaging was performed using Leica laser scanning confocal system (Leica TCS SP8X DLS confocal microscope) with a 20X objective lens. Ten µl of 50 mM KCl

or KNO_3 was loaded along one edge of the coverslip to reach a final 10 mM KCl or KNO_3. To record fluorescence images of sCiNiS, the excitation was set at 488 nm and emission was collected at 525-545 nm. The scanning resolution was set at 1024×1024 pixels for mesophyll cells and root tip cells. To obtain the dose-response curve of mesophyll cell fluorescence signal to nitrate, 10 μl of 5, 50, 500, 1,250, 5,000, and 50,000 μM KNO_3 was loaded along the edge of the coverslip to reach a final 1, 10, 100, 250, 1,000, and 10,000 μM KNO_3. Images were collected at 5 min after nitrate induction. For generating time-lapse images of fluorescence signal induced by 10 mM nitrate. The images were captured every 20 s for mesophyll cells as described above. Images were collected and processed using Leica Application Suite X software (Leica), Image J software, and Adobe Photoshop software. The signal values of sCiNiS fluorescence intensity were calculated from indicated regions. The dynamic fluorescence intensity values (Ratio) were calculated as $(F-F_0)/F_0$, where F_0 represents the starting point value. The signal ratio was produced using GraphPad Prism software.

Multiple sequence alignment for NLP

Nine NLP protein sequences of *Arabidopsis* were downloaded from TAIR (https://www.arabidopsis.org/). NLP protein sequences of other species were retrieved from Ensembl Plants (http://plants.ensembl.org/), Phytozome (https://phytozome-next.jgi.doe.gov/), FernBase (https://www.fernbase.org/) and ConGenIE (https://congenie.org/) by BLAST analysis of *Arabidopsis* NLP7. The multiple sequence alignment of all NLP proteins was performed using the online software Clustal Omega (https://www.ebi.ac.uk/Tools/msa/clustalo/), and the alignment results were edited and visualized using the Jalview (Jalview 2.11.1.4) program.

Structural prediction of NLP7 protein and the nitrate-binding domain

The NreA-NO_3^- [Protein Data Bank (PDB) code: 4IUK] crystal structure PDB file was downloaded from the protein data bank: (https://www.rcsb.org). The predicted protein structure NLP7 (Q84TH9) using RoseTTAFold was downloaded from

https://robetta.bakerlab.org/ (*32*) or using AlphaFold2 was downloaded from https://alphafold.ebi.ac.uk/ (*33*). The Pymol visualization tool (http://pymol.org/2/) was used to visualize the structure. The nitrate binding domain structure of NreA (45-97 amino acids), NLP2 (395-438 amino acids), NLP4 (345-388 amino acids), NLP5 (350-393 amino acids), NLP6 (353-396 amino acids), NLP7 (395-438 amino acids), NLP8 (397-440 amino acids), NLP9 (343-386 amino acids), *Os*NLP3 (383-426 amino acids), *Bna*NLP7 (392-435 amino acids), *Zm*NLP6 (301-344 amino acids), *Ta*NLP7 (373-416 amino acids), and *Gm*NLP6 (375-418 amino acids) were selected for comparison.

Prediction of the nuclear localization signal in NLP7

We performed the prediction of nuclear localization signal sequence in NLP7 using the cNLS Mapper tool (https://nls-mapper.iab.keio.ac.jp/cgi-bin/NLS_Mapper_form.cgi) with the following parameters: 2.0 cut-off score and search entire region.

Statistics

Statistical analyses were analyzed with GraphPad Prism 8 software. We determined the statistical significance of differences between two groups using the unpaired two-tailed Student's *t*-test and among more than two groups using one-way or two-way ANOVA analysis with Tukey's multiple comparisons. The probabilities from the statistical methods used in the main figures are presented in the figures and summarized below. Fig 1D: ****P < 0.0001 (two-way ANOVA analysis with Tukey's multiple comparisons test). Fig 1F: **P = 0.0036, ***P = 0.0003, ****P < 0.0001 (one-way ANOVA analysis with Tukey's multiple comparisons test). Fig. 2B: ****P < 0.0001 (two-way ANOVA analysis with Tukey's multiple comparisons test). Fig. 2D: ***P = 0.0003 (two-way ANOVA analysis with Tukey's multiple comparisons test). Fig. 5D: ****P < 0.0001 (two-way ANOVA analysis with Tukey's multiple comparisons test). Fig. 5F: ****P < 0.0001 (two-way ANOVA analysis with Tukey's multiple comparisons test).

Data availability

RNA-seq raw data are deposited to Gene expression Omnibus (GEO) under accession number GSE198475. The plasmids and the transgenic *Arabidopsis* seeds generated in this study are available upon request.

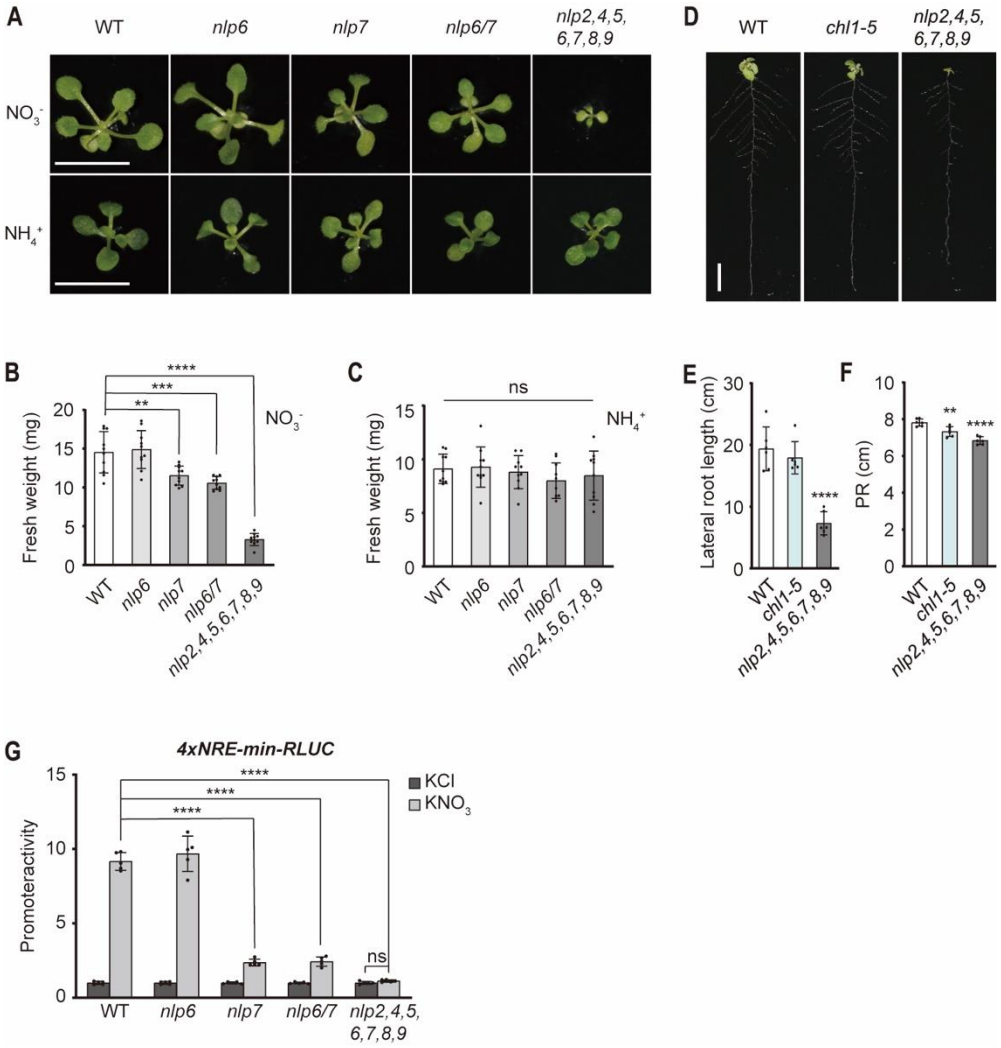

Fig. S1. Analysis of *nlp6*, *nlp7*, *nlp6,7*, *nlp2,4,5,6,7,8,9*, and *chl1-5* mutants.

(A) The *nlp2,4,5,6,7,8,9* mutant displays deficiency in nitrate-specific promotion of shoot development. Wild-type (WT), *nlp6*, *nlp7*, *nlp6,7,* or *nlp2,4,5,6,7,8,9* seedlings were germinated and grown on 2.5 mM ammonium succinate medium or 5 mM KNO_3 medium for 15 days. The images are representative of 10 seedlings. Scale bar, 1 cm. (B) (C) The average fresh weight of 15-d-old plants. WT and *nlp* mutants were grown on 5 mM KNO_3 medium (B) or 2.5 mM ammonium succinate medium (C). $^{**}P = 0.0047$, $^{***}P = 0.0003$, $^{****}P < 0.0001$(Student's *t*-test). Error bars, SD; $n = 10$ biological replicates. (D-F)

The *nlp2,4,5,6,7,8,9* mutant displays altered root architecture. WT, *chl1-5,* or *nlp2,4,5,6,7,8,9* plants were germinated on 2.5 mM ammonium succinate and then grown on a 5 mM KNO_3 medium for 8 days. The images are representative of 5

seedlings. Scale bar, 1 cm. Lateral root length (E) and primary root length (F). $^{**}P$ = 0.0043 (Student's *t-test*), $^{****}P < 0.0001$. Error bars, SD; n = 6 biological replicates. (G) Comparative analyses of 4x*NRE-min-LUC* activation by nitrate. Nitrate-free leaf cells were isolated from WT, *nlp6*, *nlp7*, *nlp6,7,* or *nlp2,4,5,6,7,8,9* plants and transfected with 4x*NRE-min-LUC*. Transfected leaf cells were incubated in WI buffer for 4 h recovery before induction by 10 mM KCl or KNO_3 for 2 h. The fold change is calculated relative to the value of the KCl treatment. $^{****}P < 0.0001$ (two-way ANOVA analysis with Tukey's multiple comparisons test). Error bars, SD; n = 5 biological replicates.

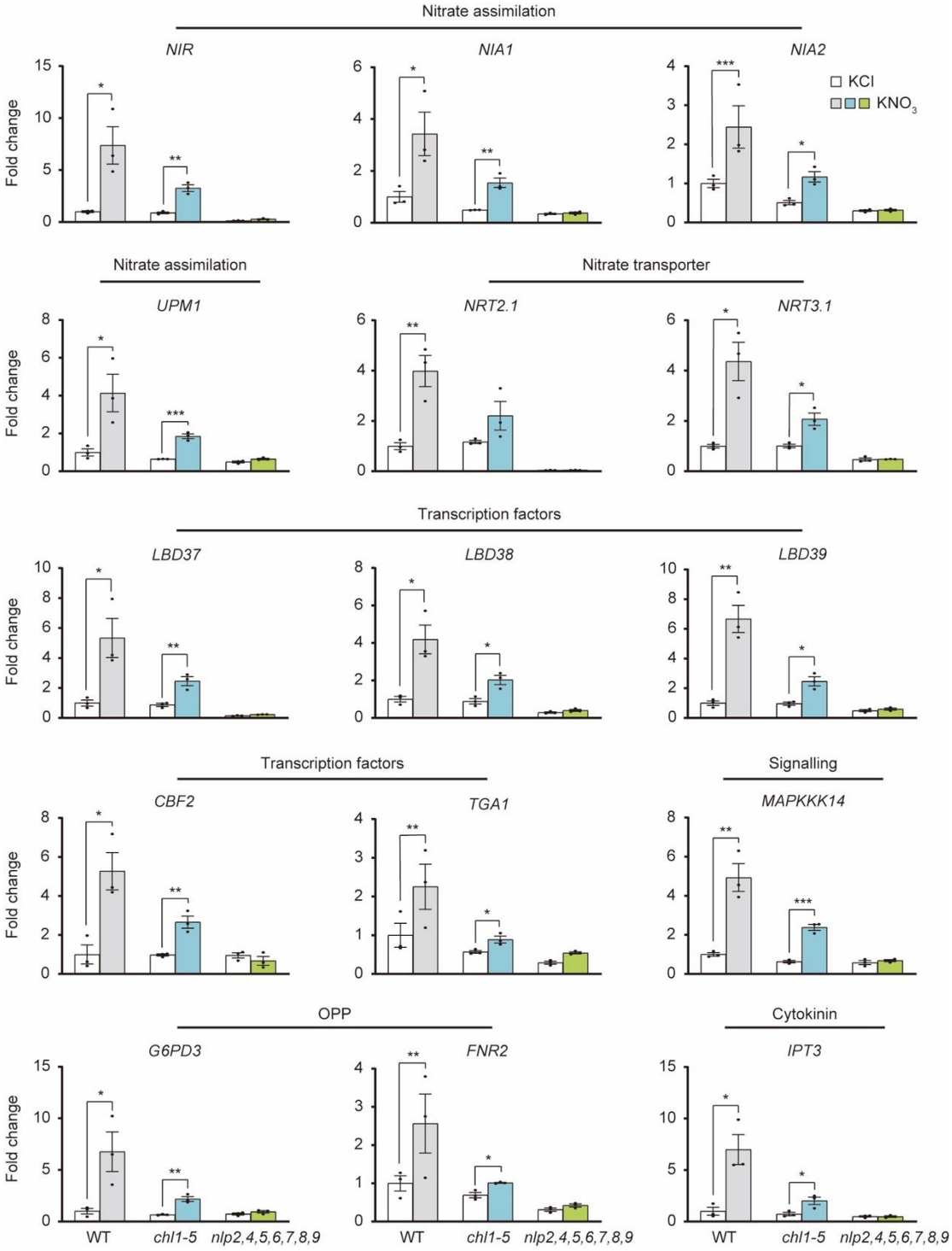

Fig. S2. Primary nitrate-responsive gene activation is abolished in *nlp2,4,5,6,7,8,9* but only diminished in *chl1-5*.

Relative fold change was calculated from RNA-seq data sets. Relative HTSeq read counts of primary nitrate response marker gene expression is normalized to that of *UBQ10*. The fold change is relative to the value of WT treated with KCl. Error bars, SD; n = 3 biological replicates. * $P < 0.05$, * $P < 0.01$ (Student's *t*-test).

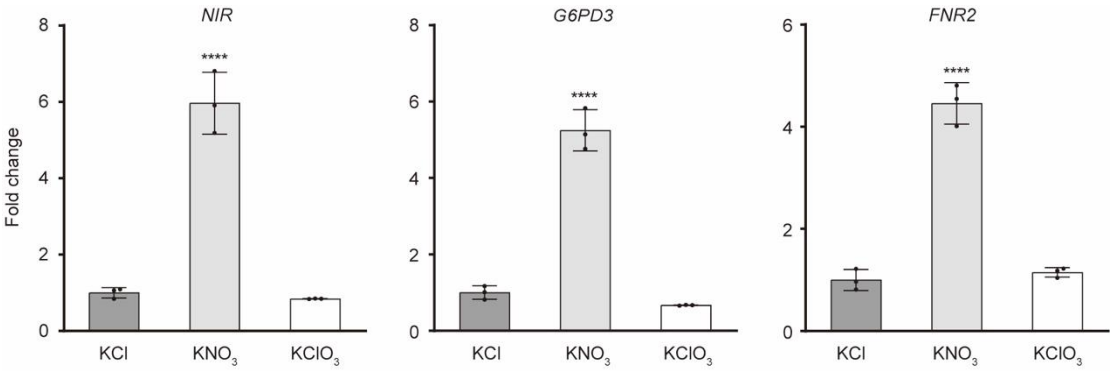

Fig. S3. Primary nitrate-responsive genes are induced by nitrate but not its analog chlorate.

RT-qPCR analyses with 7-d-old seedlings (10 mM KCl or KNO_3, 15 min). Error bars, SD; *n* = 3 biological replicates. **** $P < 0.0001$ (Student's *t*-test).

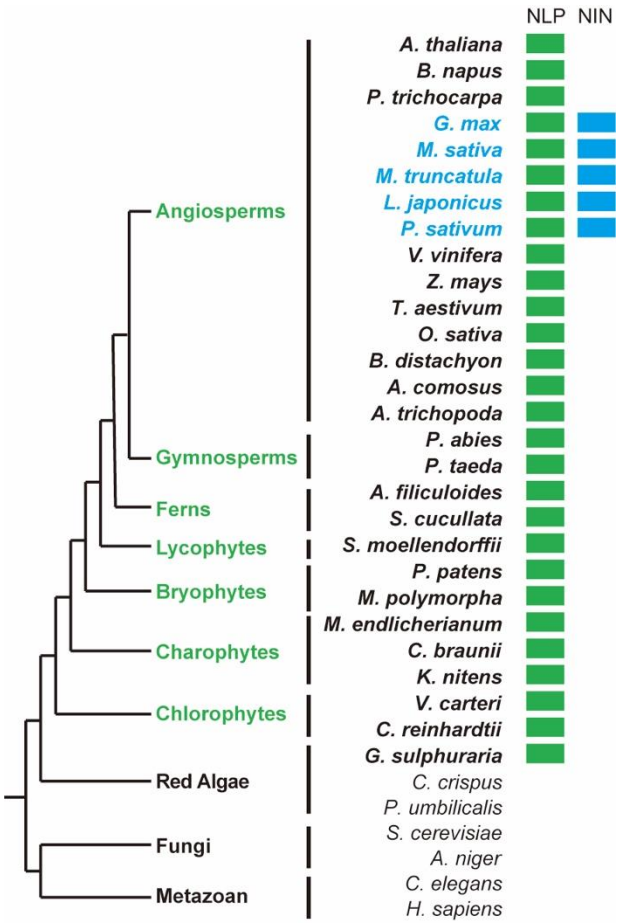

Fig. S4. The phylogenetic tree of NIN and NLP among Eukaryota.

The phylogenetic tree presents the generally accepted species in each group (*27, 45*). The taxonomic names of land plants and green algae are highlighted in green. The species that possess NLP7 orthologs are highlighted in the bold and green rectangle. Legume species that have evolved NINs later to regulate root nodulation and N_2 fixation are highlighted in a blue rectangle.

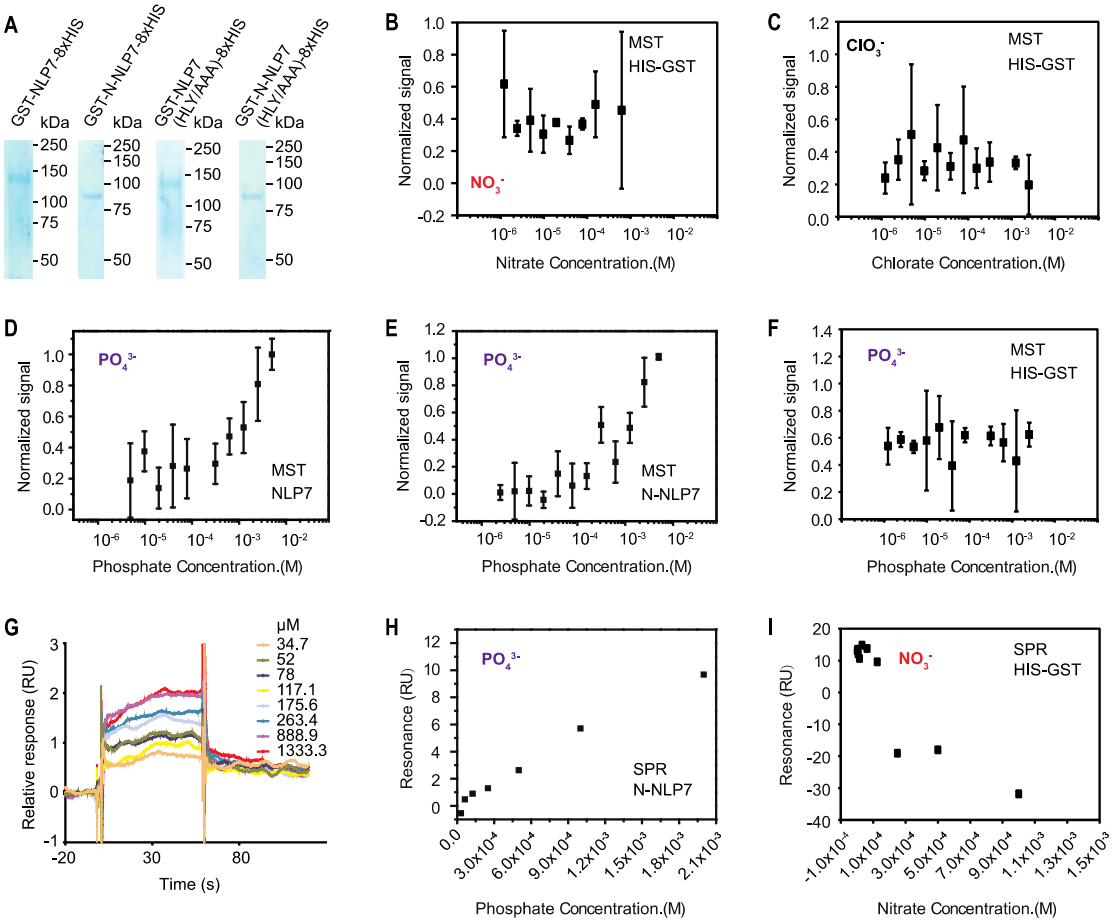

Fig. S5. Binding specificity of full-length NLP7 and N-NLP7.

(A) Purified GST-NLP7-8xHIS, GST-N-NLP7-8xHIS, GST-NLP7(HYL/AAA)-8xHIS, and GST-N-NLP7(HYL/AAA)-8xHIS proteins from *E.coli.* (B)(C) HIS-GST controls. Nitrate (B), or chlorate (C) does not bind to HIS-GST control protein using MST assays. Error bars, SD; *n* = 3 independent thermophoresis measurements. (D) Phosphate does not bind to full-length NLP7. Error bars, SD; n = 3 independent thermophoresis measurements. (E) Phosphate does not bind to N-NLP7. Error bars, SD; n = 3 independent thermophoresis measurements. (F) Phosphate does not bind to HIS-GST control protein using MST assays. Error bars, SD; *n* = 3 independent thermophoresis measurements. (G) A representative SPR sensorgram of nitrate on the N-NLP7 chip which is shown in Fig. 3C. (H) SPR analysis of phosphate-N-NLP7 interaction. N-NLP7 protein was covalently immobilized on a CM5 sensor chip and titrated with increasing phosphate concentrations. (I) HIS-GST protein does not bind to nitrate by SPR analysis. HIS-GST protein was covalently immobilized on a CM5 sensor chip and

titrated with increasing nitrate concentrations. The result is a representative of three independent experiments.

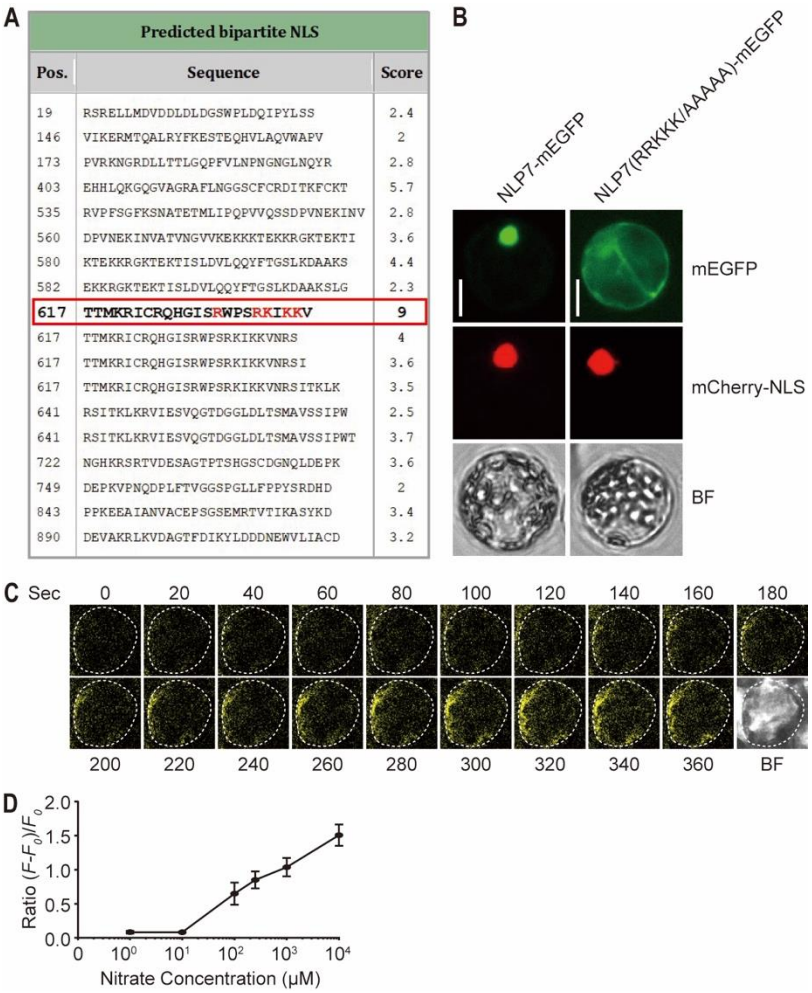

Fig. S6. Nitrate triggers sCiNiS fluorescence.

(A) Identification of nuclear localization sequences in NLP7. The predicted bipartite nuclear localization sequence (NLS) of NLP7 was obtained using the cNLS Mapper. The sequence with the highest score was selected (outlined in red) for further experimental validation. (B) NLP7(RRKKK/AAAAA)-mEGFP is localized in the cytoplasm. Leaf cells were co-transfection with mCherry-NLS as a nuclear localization control and incubated for 12 h. BF: Bright field. mCherry-NLS, nuclear HY5-mCherry. Images are representative of 16 protoplasts. Scale bars, 10 μm. (C) Time-lapse imaging of the nitrate biosensor sCiNiS in transgenic plants. The fluorescence signal in the mesophyll cells in cotyledons was induced by applying 10 mM KNO_3. Images are representative of 10 seedlings. BF: Bright field. (D) Dose-response curve of mesophyll cell fluorescence signal to nitrate.

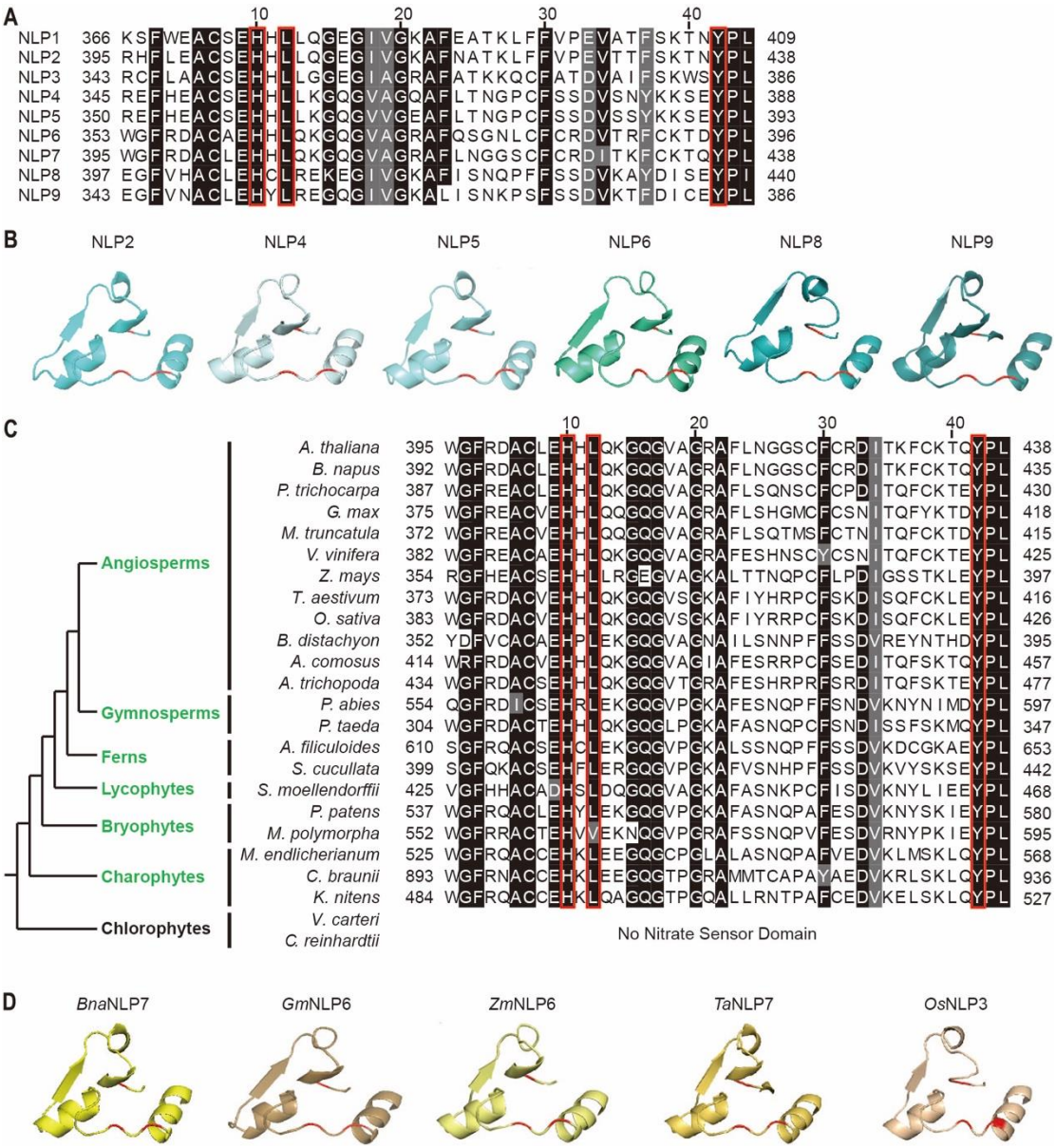

Fig. S7. The nitrate-binding domain is conserved in other NLPs and NLP7 orthologs of land plants and Charophytes.

(A) Sequence alignment of the nitrate-binding domain of *Arabidopsis* NLP proteins. The multiple sequence alignment of all NLP proteins was performed using Clustal Omega. The critical nitrate-binding residues are outlined in red. (B) Prediction of the nitrate-binding domain structure of NLP2,4,5,6,8,9 by RoseTTAfold. (C) Sequence alignment of the nitrate-binding domain of the *Arabidopsis* NLP7 orthologs retrieved from Blast analysis against NLP7 in each species. The tree represents the commonly accepted phylogenetic relations between the groups represented (*27, 45*). Numbers refer

to the amino acid positions. The critical nitrate-binding residues are outlined in red. Land plant species and green algae with the evolutionarily conserved nitrate-binding domain are colored in green. (D) Prediction of the nitrate-binding domain structure of NLP7 orthologs in major crops by RoseTTAfold. Rapeseed *Bna*NLP7, soybean *Gm*NLP6, maize *Zm*NLP6, wheat *Ta*NLP7, and rice *Os*NLP3.

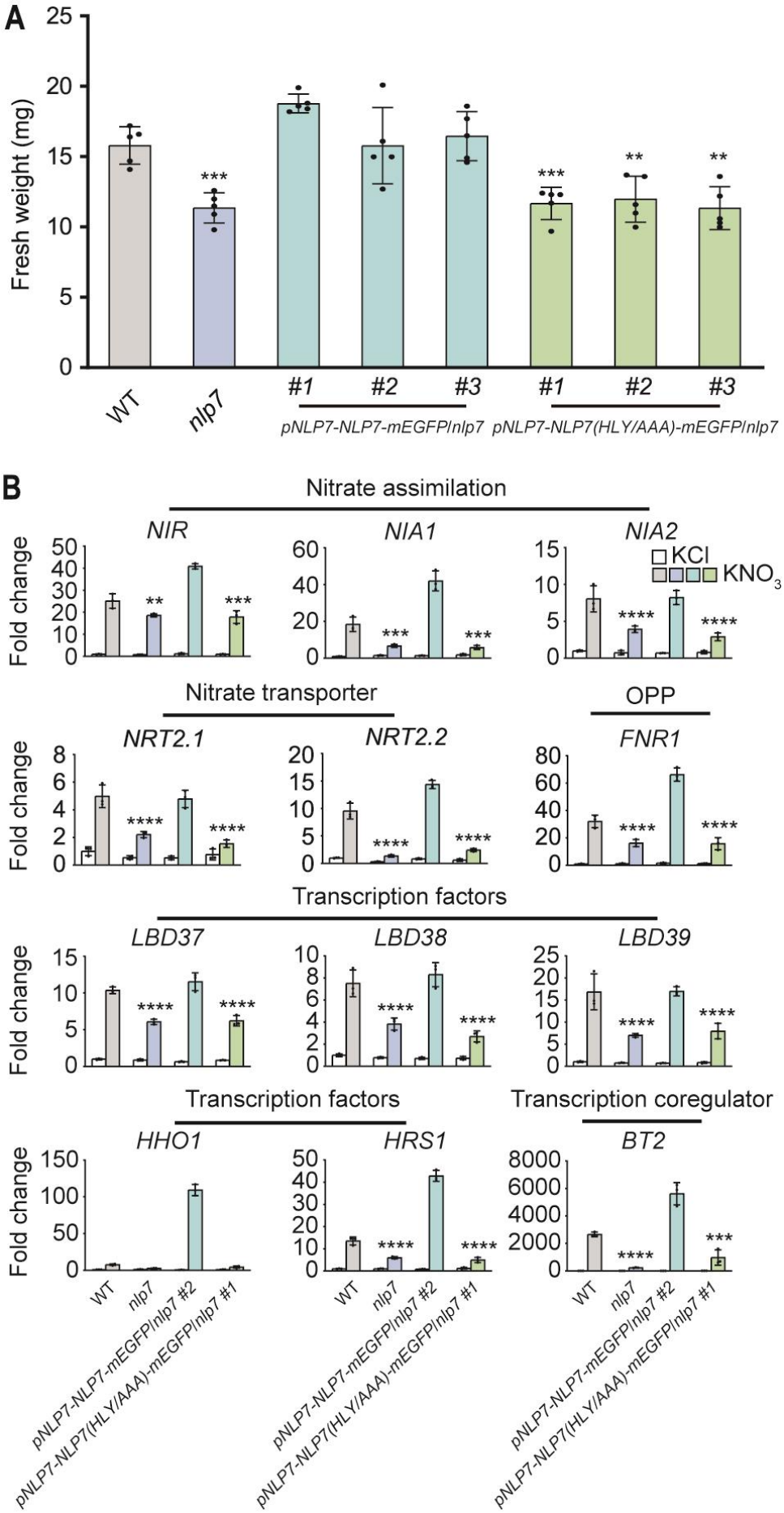
A
Fresh weight (mg)
WT
nlp7
#1
#2
#3
#1
#2
#3
pNLP7-NLP7-mEGFP/nlp7
pNLP7-NLP7(HLY/AAA)-mEGFP/nlp7
B
Nitrate assimilation
NIR
NIA1
NIA2
KCl
KNO3
Fold change
Nitrate transporter
NRT2.1
NRT2.2
OPP
FNR1
Transcription factors
LBD37
LBD38
LBD39
Transcription factors
HHO1
HRS1
Transcription coregulator
BT2
WT
nlp7
pNLP7-NLP7-mEGFP/nlp7 #2
pNLP7-NLP7(HLY/AAA)-mEGFP/nlp7 #1

Fig. S8. The nitrate-binding mutant cannot complement *nlp7*.

(A) The shoot biomass. Fresh weight was quantified in WT, *nlp7*, *pNLP7-NLP7-mEGFP*/*nlp7,* or *pNLP-NLP7(HYL/AAA)-mEGFP*/*nlp7*. ***P = 0.0004, ***P = 0.0008, **P = 0.0036, **P = 0.0011 (t-test). Error bars, SD; n = 5 biological replicates. (B) RT–qPCR analyses of primary nitrate responsive genes in WT, *nlp7*, *pNLP7-NLP7-mEGFP*/*nlp7,* or *pNLP7-NLP7(HYL/AAA)-mEGFP*/*nlp7* seedlings (10 mM KCl or KNO_3, 2h). **P < 0.01, ***P < 0.001, ****P < 0.0001 (two-way ANOVA analysis with Tukey's multiple comparisons test). Error bars, SD; n = 3 biological replicates.

References and Notes

1. A. J. Bloom, The increasing importance of distinguishing among plant nitrogen sources. *Curr. Opin. Plant Biol.* **25**, 10–16 (2015). doi:10.1016/j.pbi.2015.03.002 Medline

2. R. E. Mason, J. M. Craine, N. K. Lany, M. Jonard, S. V. Ollinger, P. M. Groffman, R. W. Fulweiler, J. Angerer, Q. D. Read, P. B. Reich, P. H. Templer, A. J. Elmore, Evidence, causes, and consequences of declining nitrogen availability in terrestrial ecosystems. *Science* **376**, eabh3767 (2022). doi:10.1126/science.abh3767 Medline

3. M. Stitt, Nitrate regulation of metabolism and growth. *Curr. Opin. Plant Biol.* **2**, 178–186 (1999). doi:10.1016/S1369-5266(99)80033-8 Medline

4. N. M. Crawford, B. G. Forde, Molecular and developmental biology of inorganic nitrogen nutrition. *Arabidopsis Book* **2002**, e0011 (2002). doi:10.1199/tab.0011 Medline

5. E. A. Vidal, J. M. Alvarez, V. Araus, E. Riveras, M. D. Brooks, G. Krouk, S. Ruffel, L. Lejay, N. M. Crawford, G. M. Coruzzi, R. A. Gutiérrez, Nitrate in 2020: thirty years from transport to signaling networks. *Plant Cell* **32**, 2094–2119 (2020). doi:10.1105/tpc.19.00748 Medline

6. Y. Y. Wang, Y. H. Cheng, K. E. Chen, Y. F. Tsay, Nitrate transport, signaling, and use efficiency. *Annu. Rev. Plant Biol.* **69**, 85–122 (2018). doi:10.1146/annurev-arplant-042817-040056 Medline

7. L. Li, K. H. Liu, J. Sheen, Dynamic nutrient signaling networks in plants. *Annu. Rev. Cell Dev. Biol.* **37**, 341–367 (2021). doi:10.1146/annurev-cellbio-010521-015047 Medline

8. A. Gaudinier, J. Rodriguez-Medina, L. Zhang, A. Olson, C. Liseron-Monfils, A.-M. Bågman, J. Foret, S. Abbitt, M. Tang, B. Li, D. E. Runcie, D. J. Kliebenstein, B. Shen, M. J. Frank, D. Ware, S. M. Brady, Transcriptional regulation of nitrogen-associated metabolism and growth. *Nature* **563**, 259–264 (2018). doi:10.1038/s41586-018-0656-3 Medline

9. L. Castaings, A. Camargo, D. Pocholle, V. Gaudon, Y. Texier, S. Boutet-Mercey, L. Taconnat, J.-P. Renou, F. Daniel-Vedele, E. Fernandez, C. Meyer, A. Krapp, The nodule inception-like protein 7 modulates nitrate sensing and metabolism in Arabidopsis. *Plant J.* **57**, 426–435 (2009). doi:10.1111/j.1365-313X.2008.03695.x Medline

10. P. Walch-Liu, B. G. Forde, Nitrate signalling mediated by the NRT1.1 nitrate transporter antagonises L-glutamate-induced changes in root architecture. *Plant J.* **54**, 820–828 (2008). doi:10.1111/j.1365-313X.2008.03443.x Medline

11. C. H. Ho, S. H. Lin, H. C. Hu, Y. F. Tsay, CHL1 functions as a nitrate sensor in plants. *Cell* **138**, 1184–1194 (2009). doi:10.1016/j.cell.2009.07.004 Medline

12. R. Wang, X. Xing, Y. Wang, A. Tran, N. M. Crawford, A genetic screen for nitrate regulatory mutants captures the nitrate transporter gene NRT1.1. *Plant Physiol.* **151**, 472–478 (2009). doi:10.1104/pp.109.140434 Medline

13. M. Konishi, S. Yanagisawa, Identification of a nitrate-responsive *cis*-element in the Arabidopsis *NIR1* promoter defines the presence of multiple *cis*-regulatory elements for nitrogen response. *Plant J.* **63**, 269–282 (2010). doi:10.1111/j.1365-313X.2010.04239.x Medline

14. L. Schauser, W. Wieloch, J. Stougaard, Evolution of NIN-like proteins in *Arabidopsis*, rice, and *Lotus japonicus*. *J. Mol. Evol.* **60**, 229–237 (2005). doi:10.1007/s00239-004-0144-2 Medline

15. M. Konishi, S. Yanagisawa, Arabidopsis NIN-like transcription factors have a central role in nitrate signalling. *Nat. Commun.* **4**, 1617 (2013). doi:10.1038/ncomms2621 Medline

16. C. Marchive, F. Roudier, L. Castaings, V. Bréhaut, E. Blondet, V. Colot, C. Meyer, A. Krapp, Nuclear retention of the transcription factor NLP7 orchestrates the early response to nitrate in plants. *Nat. Commun.* **4**, 1713 (2013). doi:10.1038/ncomms2650 Medline

17. C. Chardin, T. Girin, F. Roudier, C. Meyer, A. Krapp, The plant RWP-RK transcription factors: Key regulators of nitrogen responses and of gametophyte development. *J. Exp. Bot.* **65**, 5577–5587 (2014). doi:10.1093/jxb/eru261 Medline

18. K. H. Liu, Y. Niu, M. Konishi, Y. Wu, H. Du, H. Sun Chung, L. Li, M. Boudsocq, M. McCormack, S. Maekawa, T. Ishida, C. Zhang, K. Shokat, S. Yanagisawa, J. Sheen, Discovery of nitrate-CPK-NLP signalling in central nutrient-growth networks. *Nature* **545**, 311–316 (2017). doi:10.1038/nature22077 Medline

19. J. M. Alvarez, A.-L. Schinke, M. D. Brooks, A. Pasquino, L. Leonelli, K. Varala, A. Safi, G. Krouk, A. Krapp, G. M. Coruzzi, Transient genome-wide interactions of the master transcription factor NLP7 initiate a rapid nitrogen-response cascade. *Nat. Commun.* **11**, 1157 (2020). doi:10.1038/s41467-020-14979-6 Medline

20. M. Konishi, T. Okitsu, S. Yanagisawa, Nitrate-responsive NIN-like protein transcription factors perform unique and redundant roles in Arabidopsis. *J. Exp. Bot.* **72**, 5735–5750 (2021). doi:10.1093/jxb/erab246 Medline

21. V. Niemann, M. Koch-Singenstreu, A. Neu, S. Nilkens, F. Götz, G. Unden, T. Stehle, The NreA protein functions as a nitrate receptor in the staphylococcal nitrate regulation system. *J. Mol. Biol.* **426**, 1539–1553 (2014). doi:10.1016/j.jmb.2013.12.026 Medline

22. J. Canales, T. C. Moyano, E. Villarroel, R. A. Gutiérrez, Systems analysis of transcriptome data provides new hypotheses about *Arabidopsis* root response to nitrate treatments. *Front. Plant Sci.* **5**, 22 (2014). doi:10.3389/fpls.2014.00022 Medline

23. W. Ma, J. Li, B. Qu, X. He, X. Zhao, B. Li, X. Fu, Y. Tong, Auxin biosynthetic gene *TAR2* is involved in low nitrogen-mediated reprogramming of root architecture in Arabidopsis. *Plant J.* **78**, 70–79 (2014). doi:10.1111/tpj.12448 Medline

24. K. H. Liu, C. Y. Huang, Y. F. Tsay, CHL1 is a dual-affinity nitrate transporter of Arabidopsis involved in multiple phases of nitrate uptake. *Plant Cell* **11**, 865–874 (1999). doi:10.1105/tpc.11.5.865 Medline

25. M. Konishi, S. Yanagisawa, Roles of the transcriptional regulation mediated by the nitrate-responsive *cis*-element in higher plants. *Biochem. Biophys. Res. Commun.* **411**, 708–713 (2011). doi:10.1016/j.bbrc.2011.07.008 Medline

26. W. Suzuki, M. Konishi, S. Yanagisawa, The evolutionary events necessary for the emergence of symbiotic nitrogen fixation in legumes may involve a loss of nitrate responsiveness of the NIN transcription factor. *Plant Signal. Behav.* **8**, e25975 (2013). doi:10.4161/psb.25975 Medline

27. F. Fichtner, I. M. Dissanayake, B. Lacombe, F. Barbier, Sugar and nitrate sensing: a multi-billion-year story. *Trends Plant Sci.* **26**, 352–374 (2021). doi:10.1016/j.tplants.2020.11.006 Medline

28. J. O. Lundberg, Nitrate transport in salivary glands with implications for NO homeostasis. *Proc. Natl. Acad. Sci. U.S.A.* **109**, 13144–13145 (2012). doi:10.1073/pnas.1210412109 Medline

29. J. L. Parker, S. Newstead, Molecular basis of nitrate uptake by the plant nitrate transporter NRT1.1. *Nature* **507**, 68–72 (2014). doi:10.1038/nature13116 Medline

30. S. Q. Hutsell, R. J. Kimple, D. P. Siderovski, F. S. Willard, A. J. Kimple, High-affinity immobilization of proteins using biotin- and GST-based coupling strategies. *Methods Mol. Biol.* **627**, 75–90 (2010). doi:10.1007/978-1-60761-670-2_4 Medline

31. M. Mita, M. Ito, K. Harada, I. Sugawara, H. Ueda, T. Tsuboi, T. Kitaguchi, Green fluorescent protein-based glucose indicators report glucose dynamics in living cells. *Anal. Chem.* **91**, 4821–4830 (2019). doi:10.1021/acs.analchem.9b00447 Medline

32. M. Baek, F. DiMaio, I. Anishchenko, J. Dauparas, S. Ovchinnikov, G. R. Lee, J. Wang, Q. Cong, L. N. Kinch, R. D. Schaeffer, C. Millán, H. Park, C. Adams, C. R. Glassman, A. DeGiovanni, J. H. Pereira, A. V. Rodrigues, A. A. van Dijk, A. C. Ebrecht, D. J. Opperman, T. Sagmeister, C. Buhlheller, T. Pavkov-Keller, M. K. Rathinaswamy, U. Dalwadi, C. K. Yip, J. E. Burke, K. C. Garcia, N. V. Grishin, P. D. Adams, R. J. Read, D. Baker, Accurate prediction of protein structures and interactions using a three-track neural network. *Science* **373**, 871–876 (2021). doi:10.1126/science.abj8754 Medline

33. J. Jumper, R. Evans, A. Pritzel, T. Green, M. Figurnov, O. Ronneberger, K. Tunyasuvunakool, R. Bates, A. Žídek, A. Potapenko, A. Bridgland, C. Meyer, S. A. A.

Kohl, A. J. Ballard, A. Cowie, B. Romera-Paredes, S. Nikolov, R. Jain, J. Adler, T. Back, S. Petersen, D. Reiman, E. Clancy, M. Zielinski, M. Steinegger, M. Pacholska, T. Berghammer, S. Bodenstein, D. Silver, O. Vinyals, A. W. Senior, K. Kavukcuoglu, P. Kohli, D. Hassabis, Highly accurate protein structure prediction with AlphaFold. *Nature* **596**, 583–589 (2021). doi:10.1038/s41586-021-03819-2 Medline

34. G. Unden, S. Nilkens, M. Singenstreu, Bacterial sensor kinases using Fe-S cluster binding PAS or GAF domains for O_2 sensing. *Dalton Trans.* **42**, 3082–3087 (2013). doi:10.1039/C2DT32089D Medline

35. D. Coskun, D. T. Britto, W. Shi, H. J. Kronzucker, Nitrogen transformations in modern agriculture and the role of biological nitrification inhibition. *Nat. Plants* **3**, 17074 (2017). doi:10.1038/nplants.2017.74 Medline

36. S. D. Yoo, Y. H. Cho, J. Sheen, *Arabidopsis* mesophyll protoplasts: a versatile cell system for transient gene expression analysis. *Nat. Protoc.* **2**, 1565–1572 (2007). doi:10.1038/nprot.2007.199 Medline

37. M. Boudsocq, M. R. Willmann, M. McCormack, H. Lee, L. Shan, P. He, J. Bush, S.-H. Cheng, J. Sheen, Differential innate immune signalling via Ca^{2+} sensor protein kinases. *Nature* **464**, 418–422 (2010). doi:10.1038/nature08794 Medline

38. D. G. Gibson, L. Young, R.-Y. Chuang, J. C. Venter, C. A. Hutchison 3rd, H. O. Smith, Enzymatic assembly of DNA molecules up to several hundred kilobases. *Nat. Methods* **6**, 343–345 (2009). doi:10.1038/nmeth.1318 Medline

39. S. J. Clough, A. F. Bent, Floral dip: A simplified method for *Agrobacterium*-mediated transformation of *Arabidopsis thaliana*. *Plant J.* **16**, 735–743 (1998). doi:10.1046/j.1365-313x.1998.00343.x Medline

40. R. P. Hellens, E. A. Edwards, N. R. Leyland, S. Bean, P. M. Mullineaux, pGreen: A versatile and flexible binary Ti vector for Agrobacterium-mediated plant transformation. *Plant Mol. Biol.* **42**, 819–832 (2000). doi:10.1023/A:1006496308160 Medline

41. J. Tilsner, O. Linnik, N. M. Christensen, K. Bell, I. M. Roberts, C. Lacomme, K. J. Oparka, Live-cell imaging of viral RNA genomes using a Pumilio-based reporter. *Plant J.* **57**, 758–770 (2009). doi:10.1111/j.1365-313X.2008.03720.x Medline

42. B. De Rybel, W. van den Berg, A. Lokerse, C.-Y. Liao, H. van Mourik, B. Möller, C. L. Peris, D. Weijers, A versatile set of ligation-independent cloning vectors for functional studies in plants. *Plant Physiol.* **156**, 1292–1299 (2011). doi:10.1104/pp.111.177337 Medline

43. L. Yang, X. Wang, W. Deng, W. Mo, J. Gao, Q. Liu, C. Zhang, Q. Wang, C. Lin, Z. Zuo, Using HEK293T expression system to study photoactive plant cryptochromes. *Front. Plant Sci.* **7**, 940 (2016). doi:10.3389/fpls.2016.00940 Medline

44. R. P. Sparks, R. Fratti, Use of microscale thermophoresis (MST) to measure binding affinities of components of the fusion machinery. *Methods Mol. Biol.* **1860**, 191–198 (2019). doi:10.1007/978-1-4939-8760-3_11 Medline

45. M. Jamsheer K, S. Jindal, A. Laxmi, Evolution of TOR-SnRK dynamics in green plants and its integration with phytohormone signaling networks. *J. Exp. Bot.* **70**, 2239–2259 (2019). doi:10.1093/jxb/erz107 Medline